Research Article

Muhammad Afzal, Faiza Zahid, Badar E Alam, Mohammed M. M. Jaradat*, Imran Siddique*, Bagh Ali, and Binjian Ma

Investigating the behaviour of electro-magneto-hydrodynamic Carreau nanofluid flow with slip effects over a stretching cylinder

https://doi.org/10.1515/ntrev-2025-0166
received May 21, 2024; accepted April 8, 2025

Abstract: This study primary focus to analyses the slip flow of electro-magneto-hydrodynamic (EMHD) Carreau nanofluid across a stretching cylinder in the context of Arrhenius activation energy, chemical reactions, and variable thermal conductivity within a porous medium. To observe the effects of Brownian motion and thermophoresis, which are critical in nanofluid dynamics, Buongiorno's model is employed. Also, the effects of changing EMHD forces on fluid flow dynamics are investigated. Due to the strong Lorentz force that is produced when electric and magnetic fields interact, it is crucial to take into account their combined effects in a variety of industrial applications. By introducing nonsimilarity variables, the partial differential equations are transformed into a system of coupled ordinary differential equations (ODEs). The *bvp4c* solver, a MATLAB built-in solver, is implemented to compute the solution to the resultant set of ODEs. Graphs demonstrate how various parameters influence the profiles of velocity, microorganisms, concentration, and temperature. It is observed that thermophoresis significantly influences the thermal and concentration boundary layer regions. Skin friction increases as the curvature parameter value is enhanced. The local Nusselt number rises as the Prandtl number value increases. The local Sherwood number increases with the constant thermophoresis and the Schmidt number increases. As the curvature parameter, bioconvection Schmidt number rises and the value of local motile density increases.

Keywords: Carreau nanofluid, EMHD, variable thermal conductivity, permeable medium, chemical reaction, slip boundary condition, stretching cylinder, *bvp4c*

*** Corresponding author: Mohammed M. M. Jaradat,** Department of Mathematics and Statistics, College of Arts and Sciences, Qatar University, 2713, Doha, Qatar, e-mail: mmjst4@qu.edu.qa
*** Corresponding author: Imran Siddique,** Department of Mathematics, University of Sargodha, Sargodha 40100, Pakistan; Mathematics in Applied Sciences and Engineering Research Group, Scientific Research Center, Al-Ayen University, Nasiriyah, 64001, Iraq, e-mail: imransmsrazi@gmail.com
Muhammad Afzal: Department of Mathematics, Division of Science and Technology, University of Education, Lahore 54770, Pakistan
Faiza Zahid: Department of Mathematics, National University of Sciences and Technology, Islamabad 44000, Pakistan; Poznan University of Technology, Institute of Structural Analysis, Poznan, Poland
Badar E Alam: Department of Physics and Mathematics, Iberoamerican University of Mexico City, Paseo de Reforma 880, Lomas de Santa Fe, Mexico City, 01219, Mexico City, Mexico
Bagh Ali, Binjian Ma: School of Mechanical Engineering and Automation, Harbin Institute of Technology, Shenzhen 518055, China

Nomenclature

b	chemotaxis constant (m)
C	nanoparticles volume fraction (–)
C_∞	ambient nanoparticle volume fraction (–)
Cp	specific heat (J kg^{-1} K^{-1})
D_B	Brownian diffusion coefficient (m^2 s^{-1})
D_m	microorganism diffusion coefficient (m^2 s^{-1})
k_r	rate of chemical reaction (mol m^{-1} s^{-1})
m	fitted rate constant (–)
M	magnetic parameter
n	power law index (–)
N_∞	ambient nanoparticle volume fraction (–)
Nu_x	Nusselt number
Pr	Prandtl number
q_r	radiative heat flux (W s^{-2})
T	nondimensional temperature (K)
T_w	temperature at bottom disk (K)
T_∞	ambient temperature (K)
W_c	swimming speed of micro-organism (m s^{-1})
(u, v)	velocity components
ν	kinematic viscosity (m^{-2} s^{-1})
ρ	density of fluid (kg m^{-3})
κ	thermal conductivity of fluid (W m^{-1} K^{-1})
σ	fluid electrical conductivity (kg^{-1} m^3 A^2)

α thermal diffusivity ($m^2\ s^{-1}$)
η dimensionless distance (–)
κ_1 permeability of the porous medium (m^2)

1 Introduction

Recent research over the past few decades highlights the growing interest in the study of non-Newtonian fluids within the field of fluid dynamics. Non-Newtonian fluid flows find extensive applications in industrial and manufacturing processes [1], including the creation of insulating materials, extrusion, hot rolling, metal spinning, and metal extrusion. Moreover, integrating heat transfer with stretching flow concepts is crucial for enhancing the efficiency of these applications [2,3]. Shear rate and shear stress have a nonlinear connection in non-Newtonian fluids. From the modelling point of view, the Carreau model is fundamental since it illustrates power-law behaviour and is frequently employed as a core predictive method. The Carreau model is a four-parameter one first put forth by Carreau [4] in 1972 and was developed in a series of many different research works. Gomathi and De investigated the effect of ion slip on the dynamics of Casson-Williamson flow and reported that an increase in viscous forces, combined with yield stress, leads to a reduction in fluid velocity [5]. In the study by Raju and Sandeep [6], the researchers conducted a study on magneto-hydrodynamic (MHD) Carreau fluid using cross-diffusion over a wedge. They observed that with an increase in wedge angle parameter, the velocity field of fluid also increases. Using different flow configuration, many other researchers focus on dynamics of various non-Newtonian fluid subject to different physical conditions [7–11]. Raju and Sandeep [12] conducted a comprehensive investigation of the effects of an uncertain heat source or sink and nonlinear thermal radiation in the presence of both homogeneous and heterogeneous phenomena. They extensively studied and analysed the implications of these factors on the heat transfer characteristics and behaviour of the system. The Buongiorno model was used by Khan *et al.* [13] to predict the behaviour of a time-dependent Carreau fluid along a wedge. They discovered that increasing the Weissenberg number raises temperature of the fluid.

A fluid and nanoparticles are combined to form a nanofluid. In nanofluids, nanoparticles are frequently formed of metals, oxides, carbides, and carbon nanotubes. Compared to their respective base fluids, nanofluids have very distinct thermophysical characteristics. Numerous industries [14], including cooling of transformer oil, cooling of electronics, residential refrigerators and freezers, solar water heating, and engine cooling, use nanofluids [15–17]. In an experiment conducted few years ago, Choi and Eastman [18] and Choi *et al.* [19] introduced nanoparticles to a base fluid and looked at the thermophysical properties of the nanofluids in comparison to the base fluids. He found that the efficiency of nanofluids is improved, especially in terms of their thermal conductivity, which is much higher than that of the base fluid. Numerous scholars have engaged in theoretical and experimental works in this area since this ground-breaking experiment [9,20,21]. Microbes residing in a fluid are responsible for the occurrence of bioconvection, a phenomenon that plays a role in stabilising nanoparticles and increasing the fluid's susceptibility to thermal and mass transport. This aspect has been studied by Kuznetsov [22]. Fields such as biomedical engineering, biological technology, and environmental systems rely on the suspension of nanoparticles and bioconvection, as highlighted by Chan *et al.* [23].

Static charges provide an electric field, whereas the changing motion of electric charges produces a magnetic field. MHD is the study of magnetic properties and dynamics of electrically conducting fluids. In the disciplines of engineering, transportation, and medical sciences, MHD has a broad spectrum of applications. For instance, a strong electric field could be used to control or halt the development of a brain tumour. The research conducted by Sparrow and Cess [24] presented a mathematical model that elucidates the behaviour of free convective flow in the presence of a magnetic field. The study focused on examining the specific characteristics of MHD flow under forced and free convective conditions between two parallel plates. The study conducted by Mazumder *et al.* [25] revealed that Hall currents have a substantial impact on heat transfer characteristics and flow. The research conducted by Raptis [26] focused on analysing the dynamics of unsteady convective flow through a porous medium. In their numerical investigation, Rudraiah *et al.* [27] examined the natural convective fluid flow within a rectangular enclosure. They observed that the impact of a magnetic field on the rate of heat transfer is more pronounced in a section with a small Grashof number. Certainly, the study carried out by AboEldahab [28] focused on examining the heat transfer characteristics of free convection MHD flow as it passes a stretching sheet. The analysis took into consideration the impact of radiation and buoyancy effects on flow and heat transfer phenomena in this context. Awais *et al.* [29] made notable observations regarding the dynamics of MHD Sisko fluid flowing towards a stretching cylinder. They discovered that velocity and temperature are affected differently depending on the magnetic field's strength. As a result of the heating effect caused by the magnetic field, they specifically observed a drop in velocity and a rise in temperature. The movement of the electrically conducting fluids is influenced

by an external magnetic field [30]. A Lorentz force results from this interaction.

The electric field [31] generates the strong Lorentz force needed for flow control in industrial applications, and Sajid and Hayat [32] examined the impact of heat radiation on boundary layer flow caused by an exponentially stretched sheet. Shehzad *et al.* [33] examined the 3D flow properties of an Oldroyd-B fluid with a heat source, a heat sink, and varying thermal conductivity. In the studies conducted by Waqas *et al.* [34] and Dogonchi and Ganji [35] the characteristics of heat transfer mechanisms are examined with respect to variable thermal conductivity and heat source/sink. Akbar *et al.* [36] observed and investigated the effects of heat transfer on a vertical stretching plate. The study considered the influence of variable thermal conductivity and ohmic heating on heat transmission outcomes. The least amount of energy necessary for reactants to go through a chemical reaction or physical transport is called activation energy. Due to its many uses in compound innovation, geothermal artificial lakes, the recovery of thermal lubricant, and the simmering of atomic reactors, Arrhenius energy with mass transport phenomena and chemical reactions has been extensively studied. It might be challenging to calculate the activation energy using the Arrhenius equation when the temperature varies greatly with the rate constant. Since conversions can have a variety of impacts on reactants, it is imperative to be efficient with the reaction and minimize energy waste. In their experimental study [37], they focused on the convection flow of heat transmission through the combination of chemical reactions and thermal radiation. By analysing the obtained experimental data, they successfully developed a fouling resistance-based model for heat transfer. Khan *et al.* [38] examined how the cone and plate in a porous medium promoted the formation of chemically reactive species and mixed convection at the MHD Williamson nanofluid.

Based on the aforementioned discussion, the primary aim of this study is to investigate the effects of changing electro-magneto-hydrodynamic (EMHD) forces on fluid flow dynamics in the slip flow of an EMHD bioconvective Carreau nanofluid over a stretching cylinder within a porous medium. In addition, the study incorporates factors such as chemical reactions, Arrhenius activation energy, and variable thermal conductivity. Microorganisms are responsible for the occurrence of bioconvection, a phenomenon that plays a role in stabilising nanoparticles and increasing the fluid's susceptibility to thermal and mass transport. The existing literature indicates that the current constructed problem has not yet been thoroughly investigated. The outcomes of this research hold significant relevance and practical implications across multiple industries. Specifically, fields such as metallurgical procedures, blow moulding, glass fibres, and extrusion processes can benefit from the findings and insights derived from this study. A wise scope of nanofluid and non-Newtonian fluids motivated us to investigate present elaborated problem. The objective of this report is to find the answer of these questions:

- What do Arrhenius activation energy, chemical reactions, and variable thermal conductivity within a porous medium have to influence dynamics of Carreau nanofluid?
- What is the variation in quantities of engineering interest against involved physical involved parameters, to optimise the thermal management?
- What is the role of nanoparticles thermophoresis inside the Carreau nanofluid?

The content of this article is organised as follows: Section 1 presents a detailed review of the relevant literature and the research gap. Section 2 and 3 outline the mathematical modelling and governing equations and quantities of engineering interest. Section 4 explains the numerical method employed to solve the equations. Section 5 discusses the results obtained and provides a comprehensive analysis of the findings. Finally, Section 6 concludes the study, summarising the key outcomes and suggesting potential areas for future research.

2 Mathematical formulation

By incorporating thermal radiation, Arrhenius activation energy, variable thermal conductivity, and slip boundary conditions and zero mass boundary conditions, we investigate a two-dimensional electromagnetic hydrodynamics (EMHD) system where a Carreau bio-nanofluid slip flows steadily over a stretching cylinder. In our analysis, we examine the incompressible flow of a viscous fluid while taking into account the simultaneous presence of an applied magnetic field B and an electric field E. The surface is located at $r = 0$, variable magnetic field $B(x) = \frac{B_* x}{l}$, and variable electric field $E(x) = \frac{E_* x}{l}$ has been applied orthogonally to the fluid flow. It is considered that the stretching velocity in the x-direction is $u_w = \frac{ax}{L}$. The magnetic Reynolds number is of such a low magnitude that it does not generate a significant magnetic field. In Figure 1, the cylindrical axis is aligned along the x-axis, while the radial direction is represented by the r-axis.

The expression for the stress tensor of Cauchy in the case of a Carreau fluid is expressed by:

$$\ddot{\tau} = \acute{\mu}\hat{A}, \tag{1}$$

$$\frac{\acute{\mu} - \acute{\mu}_{\infty}}{\acute{\mu}_0 - \acute{\mu}_{\infty}} = [1 + (\Gamma\check{\gamma})^2]^{\frac{n-1}{2}}. \tag{2}$$

The parameter $\acute{\mu}_{\infty}$ corresponds to the viscosity at an infinite shear rate. The term $\acute{\mu}_0$ represents the viscosity at a zero shear rate. The symbol $\acute{A}$ refers to the first kind Rivlin-Erickson tensor. Γ represents a material time constant. The variable $\acute{\mu}$ denotes the shear-rate viscosity [39,40]:

$$\acute{A} = \nabla V + (\nabla V)^T, \tag{3}$$

$$\check{\gamma} = \sqrt{\frac{1}{2}\sum_i\sum_j \check{\gamma}_{ij}\check{\gamma}_{ij}} = \sqrt{\frac{1}{2}\prod} = \sqrt{\frac{1}{2}tr(\acute{A}^2)}. \tag{4}$$

The second invariant strain tensor is $\prod$. For simplification of research, we assumed $\ddot{\eta}_{\infty} = 0$ and $\Gamma\check{\gamma} < 1$ and can be defined thus by using binomial expansion equation (2) as follows:

$$\acute{\mu} = \acute{\mu}_{\circ}\left[1 + \frac{n-1}{2}(\Gamma\check{\gamma})^2\right]. \tag{5}$$

Equation (1) can be rewritten as follows:

$$\ddot{\tau} = \acute{\mu}_{\circ}\left[1 + \frac{n-1}{2}(\Gamma\check{\gamma})^2\right]\acute{A}. \tag{6}$$

For a Carreau nanofluid, the variable thermal conductivity can be described as follows:

$$\kappa(T) = \kappa_{\infty}(1 + \varepsilon\theta).$$

The equations governing are given as as follows [41–44]:

$$\frac{\partial(ru)}{\partial x} + \frac{\partial(rv)}{\partial r} = 0, \tag{7}$$

$$\begin{aligned} u\frac{\partial u}{\partial x} + v\frac{\partial u}{\partial r} &= v\frac{\partial^2 u}{\partial r^2} + v\frac{1}{r}\frac{\partial u}{\partial r} + v\frac{3\Gamma^2(n-1)}{2} \\ &\times \left(\frac{\partial u}{\partial r}\right)^2\frac{\partial^2 u}{\partial r^2} + v\frac{\Gamma^2(n-1)}{2r}\left(\frac{\partial u}{\partial r}\right)^3 \\ &- \frac{\sigma}{\rho}(B_*^2(x)u - E_*(x)B_*(x)) - \frac{v}{\kappa_1}u, \end{aligned} \tag{8}$$

$$\begin{aligned} u\frac{\partial T}{\partial x} + v\frac{\partial T}{\partial r} &= \frac{1}{\rho C_p}\frac{1}{r}\left[\frac{\partial}{\partial r}\left[\kappa(T)r\frac{\partial T}{\partial r}\right]\right] \\ &+ \tau\left[D_B\frac{\partial C}{\partial r}\frac{\partial T}{\partial r} + \frac{D_T}{T_{\infty}}\left(\frac{\partial T}{\partial r}\right)^2\right] \\ &- \frac{1}{\rho C_p r}\frac{\partial r q_r}{\partial r} + \frac{Q_1(T - T_{\infty})}{\rho C_p}, \end{aligned} \tag{9}$$

$$\begin{aligned} u\frac{\partial C}{\partial x} + v\frac{\partial C}{\partial r} &= D_B\frac{\partial^2 C}{\partial r^2} + \frac{D_B}{r}\frac{\partial C}{\partial r} + \frac{D_T}{T_{\infty} r}\frac{\partial T}{\partial r} \\ &+ \frac{D_T}{T_{\infty}}\frac{\partial^2 T}{\partial r^2} - \kappa_r(C - C_{\infty})\left(\frac{T}{T_{\infty}}\right)^m \exp\left(\frac{-E_a}{\kappa_b T_{\infty}}\right), \end{aligned} \tag{10}$$

$$u\frac{\partial N}{\partial x} + v\frac{\partial N}{\partial r} + \frac{bW_C}{(C_w - C_{\infty})}\left[\frac{\partial}{\partial r}\left[N\frac{\partial C}{\partial r}\right]\right] = \frac{D_m}{r}\frac{\partial}{\partial r}\left[r\frac{\partial N}{\partial r}\right], \tag{11}$$

where u and v are velocity components, ν is the kinematic viscosity, n is the power law index, g is the gravitational field, κ_1 is the porosity, σ is the electrical conductivity, ρ is the fluid density, T_{∞} is the ambient temperature, T is the temperature, T_w is the temperature at wall, α is the thermal conductivity, C_p is the specific heat, q_r is the thermal radiation, Q_1 is the heat source,

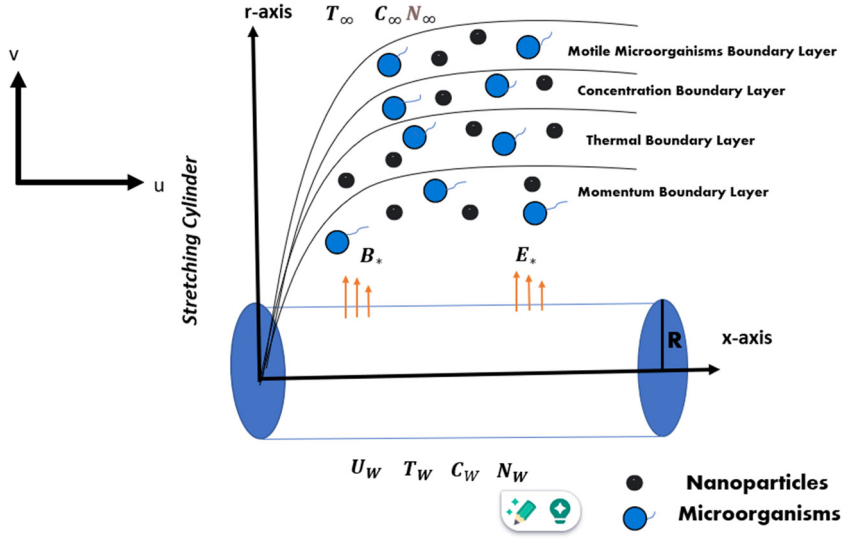

Figure 1: Problem geometry.

C is the concentration, D_T is the thermophoretic diffusion, C_w is a concentration at the wall, C_∞ is the ambient concentration, N is the concentration of microorganisms, N_w is the concentration of microorganisms at the wall, N_∞ is the ambient concentration of microorganisms, κ_r is the chemical reaction rate, m is the fitted rate constant, D_B is the Brownian diffusion, D_m is the microorganism diffusivity, W_C is the swimming speed of maximum cell, and b is the chemotaxis constant. The thermal radiation is approximated by the Rosseland model as follows [45]:

$$\frac{\partial q_r}{\partial r} = \frac{-16\sigma_* T_\infty^3}{3\kappa^*}\frac{\partial^2 T}{\partial r^2}, \tag{12}$$

where κ^* is the mean absorption coefficient and σ_* is Stefan-Boltzmann constant. The boundary conditions as follows [46,47]:

$$\begin{aligned} &u = u_w + u_{\text{slip}} = \frac{u_0 x}{l} + l_0\frac{\partial u}{\partial r}\left(1 + \frac{n-1}{2}\Gamma^2\left(\frac{\partial u}{\partial r}\right)^2\right),\\ &T = T_w + l_2\frac{\partial T}{\partial r}, \quad v = 0,\\ &D_B\frac{\partial C}{\partial r} + \frac{D_\infty}{T_\infty}\frac{\partial T}{\partial r} = 0, \quad N = N_w \quad \text{at } r = R, \end{aligned} \tag{13}$$

$$u \to 0, \quad T \to T_\infty, \quad C \to C_\infty, \quad N \to N_\infty, \quad \text{as } r \to \infty. \tag{14}$$

The similarity transformations are defined as follows [44,46]:

$$\begin{aligned} &\xi = \sqrt{\frac{u_0}{lv}}\left(\frac{r^2 - R^2}{2R}\right), \quad \Psi(\xi) = \sqrt{\frac{vu_0}{l}}xRf(\xi),\\ &u = \frac{1}{r}\frac{\partial \Psi}{\partial r}, \quad v = -\frac{1}{r}\frac{\partial \Psi}{\partial x}, \quad \theta(\xi) = \frac{T - T_\infty}{T_w - T_\infty},\\ &\chi(\xi) = \frac{N - N_\infty}{N_w - N_\infty}, \quad \phi(\xi) = \frac{C - C_\infty}{C_w - C_\infty}. \end{aligned} \tag{15}$$

In view of equation (15), the governing system of equations (7) and (14) is expressed as follows:

$$\begin{aligned} &(1 + 2\zeta\xi)f''' + 2\zeta f'' + \frac{3(n-1)}{2}\text{We}^2(1 + 2\zeta\xi)\\ &\times (f'')^2((1 + 2\zeta\xi)f'''(\xi) + \zeta f''(\xi))\\ &+ \frac{(n-1)}{2}\text{We}^2(1 + 2\zeta\xi)\zeta(f''(\xi))^3 - (f'(\xi))^2\\ &+ f(\xi)f''(\xi) - M_1^2(f'(\xi) - F) - K_p f'(\xi) = 0, \end{aligned} \tag{16}$$

$$\begin{aligned} &(1 + 2\zeta\xi)((1 + \varepsilon\theta)\theta'' + \varepsilon\theta'^2)\\ &+ (1 + \varepsilon\theta)2\zeta\theta' + (1 + 2\zeta\xi)\text{Pr}(\text{Nt}(\theta')^2 + \text{Nb}\theta'\phi')\\ &+ \text{Pr}(f\theta' + Q\theta) + \frac{4}{3}\text{Rd}((1 + 2\zeta\xi)\theta'' + \zeta\theta') = 0, \end{aligned} \tag{17}$$

$$\begin{aligned} &(1 + 2\zeta\xi)\phi'' + 2\zeta\phi' + \text{Sc}f\phi' + \frac{\text{Nt}}{\text{Nb}}(2\zeta\theta' + (1 + 2\zeta\xi)\theta'')\\ &- \text{Sc}\gamma_r(1 + \delta\theta)^m\phi\exp\left(\frac{-E_2}{(1 + \delta\theta)}\right) = 0, \end{aligned} \tag{18}$$

$$\begin{aligned} &(1 + 2\zeta\xi)\chi'' + 2\zeta\chi' + \text{Sb}f\chi' - \text{Pe}((1 + 2\zeta\xi)(\phi'\chi'\\ &+ (\chi + \delta_1)\phi'') + (\chi + \delta_1)\zeta\phi') = 0, \end{aligned} \tag{19}$$

with boundary conditions:

$$\begin{aligned} &f(0) = 0, \quad f'(0) = 1 + h_1 f''(0)\left(1\right.\\ &\left. + \frac{n-1}{2}\text{We}^2(f''(0))^2\right),\\ &f'(\infty) = 0, \quad \theta(0) = 1 + h_2\theta'(0), \quad \theta(\infty) = 0,\\ &\text{Nb}\phi'(0) + \text{Nt}\theta'(0) = 0, \quad \phi(\infty) = 0, \quad \chi(0) = 1,\\ &\chi(\infty) = 0, \end{aligned} \tag{20}$$

where $\zeta = \frac{1}{R}\sqrt{\frac{vl}{u_0}}$ is the curvature parameter, $M_1^2 = \frac{\sigma B_*^2 l}{\rho u_0}$ is a magnetic parameter, $E = \frac{E_*}{B_* u_w^2}$ refers to the electric parameter, $Q = \frac{lQ_1}{\rho u_0 C_p}$ depicts the heat generation parameter, $K_p = \frac{vl}{\kappa_1 u_0}$ is the porosity parameter, $\text{We}^2 = \frac{\Gamma^2 x^2 u_0^3}{vl^3}$ is the Weissenberg number, $E_2 = \frac{E_a}{\kappa_b T_\infty}$ represents the activation parameter, $\text{Rd} = \frac{4\sigma^* T_\infty^3}{\kappa^* \kappa}$ depicts the radiation parameter, $\text{Nb} = \frac{\tau D_B(C_w - C_\infty)}{v}$ depicts the Brownian parameter, $\text{Nt} = \frac{\tau D_T(T_w - T_\infty)}{vT_\infty}$ depicts dimensionless thermophoresis constant, $\gamma_r = \frac{\kappa_r l}{u_0}$ is the dimensionless parameter of chemical reaction, $\text{Pr} = \frac{\alpha}{v}$ depicts the Prandtl number, $\text{Sc} = \frac{v}{D_B}$ depicts the Schmidt number, $\delta_1 = \frac{N_w}{N_w - N_\infty}$ depicts the microorganism difference dimensionless parameter, $E_1 = \frac{-E_a}{\kappa_b T_\infty}$, $\text{Sb} = \frac{v}{D_m}$ depicts the dimensionless bioconvection Schmidt number, $\text{Pe} = \frac{bW_c}{D_m}$ denotes the dimensionless Peclet number, $\text{Bi} = \frac{h_f}{k}\sqrt{\frac{vl}{a}}$ depicts the Biot number, $h_1 = l_0\sqrt{\frac{u_0}{lv}}$ is the slip velocity parameter, $h_2 = l_1\sqrt{\frac{u_0}{lv}}$ is the slip temperature parameter, and $\delta = \frac{T_w - T_\infty}{T_\infty}$ depicts the temperature difference.

3 Physical characteristics

3.1 Skin friction coefficient

Frictional drag on a surface is defined by the dimensionless factor C_f. It is described as follows:

$$C_f = \frac{\ddot{\tau}_w}{2\rho u_w^2}. \tag{21}$$

The term for shear stress is:

$$\ddot{\tau}_w = \hat{\mu}\left(\frac{\partial u}{\partial r} + \frac{\Gamma^2(n-1)}{2}\left(\frac{\partial u}{\partial r}\right)^3\right)_{r=R}, \tag{22}$$

By adding the aforementioned equation to equation (21), we obtain

$$\frac{C_f(\mathrm{Re}_x)^{-\frac{1}{2}}}{2} = f''(0) + \frac{(n-1)}{2}\mathrm{We}^2(f''(0))^3, \tag{23}$$

where Re_x stands for the local Reynolds number, which is $\mathrm{Re}_x = \frac{u_w x}{\nu}$.

3.2 Local Nusselt number

To examine the heat transmission rate at the wall, Nu_x is defined as follows:

$$\mathrm{Nu}_x = \frac{x\hat{q}_w}{\kappa(T_w - T_\infty)}. \tag{24}$$

At the wall, Fourier's law is defined as follows:

$$\hat{q}_w = -\kappa\left(\frac{\partial T}{\partial r}\right)_{r=R} + (q_r)_{r=R}. \tag{25}$$

By adding the aforementioned equation to equation (24), we obtain

$$\mathrm{Nu}_x(\mathrm{Re}_x)^{-\frac{1}{2}} = -\left(1 + \frac{4}{3}\mathrm{Rd}\right)\theta'(0). \tag{26}$$

3.3 Local Sherwood number

The local Sherwood number Sh_x is determined as follows:

$$\mathrm{Sh}_x = \frac{x\hat{j}_w}{D_B(C_w - C_\infty)}. \tag{27}$$

By applying Fick's law, the mass transfer can be represented as follows:

$$\hat{j}_w = -D_B\left(\frac{\partial C}{\partial r}\right)_{r=R}. \tag{28}$$

By adding the aforementioned equation to equation (28), we obtain

$$\mathrm{Sh}_x(\mathrm{Re}_x)^{-\frac{1}{2}} = -\phi'(0). \tag{29}$$

.

3.4 Local density of motile microorganisms

The local density of motile microorganisms is given as follows:

$$\mathrm{Nn}_x = \frac{x\hat{i}_w}{D_m N_W - N_\infty}. \tag{30}$$

$$\hat{i}_w = -D_m\left(\frac{\partial N}{\partial r}\right)_{r=R}. \tag{31}$$

By adding the aforementioned equation to equation (30), we obtain

$$\mathrm{Nn}_x(\mathrm{Re}_x)^{-\frac{1}{2}} = -\chi'(0). \tag{32}$$

4 Numerical approach

In the realm of engineering and scientific simulations, complex and higher-order differential equations find frequent application. Various mathematical approaches are available in the current literature for implementation in computational simulations. Achieving high precision and efficiency, the dimensionless observations (16)–(19) and boundary conditions (20) can be effectively addressed using the *bvp4c* solver provided by MATLAB's computational tool. The utilisation of this technique is reliable, very smooth, and simple. For this present elaborated model of Carreau nanofluid across a stretching cylinder in the context of Arrhenius activation energy, chemical reactions, and variable thermal conductivity within a porous medium, the *BVP4'c* choice is motivated by its an excellent performance in accuracy and stability to solve ordinary differential equations (ODEs) [48]. To begin the process, the coupled nonlinear ODEs are initially transformed into first-order representations to facilitate the utilisation of the given equation:

$f = \mathrm{Y}_1$, $f' = \mathrm{Y}_1' = \mathrm{Y}_2$, $f'' = \mathrm{Y}_2' = \mathrm{Y}_3$, $\theta = \mathrm{Y}_4$, $\theta' = \mathrm{Y}_4' = \mathrm{Y}_5$, $\phi = \mathrm{Y}_6$, $\phi' = \mathrm{Y}_7$, $\chi = \mathrm{Y}_8$, $\chi' = \mathrm{Y}_8' = \mathrm{Y}_9$,

$$\begin{aligned}\mathrm{Y}_3' = &\left(\frac{1}{(1+2\zeta\xi) + \frac{3(n-1)}{2}(1+2\zeta\xi)^2\mathrm{We}^2(\mathrm{Y}_3)^2}\right)\\ &\times\left(-2\zeta\mathrm{Y}_3 - \frac{(n-1)}{2}\mathrm{We}^2\zeta(1+2\zeta\xi)(\mathrm{Y}_3)^3\right)\\ &- \frac{3(n-1)}{2}\mathrm{We}^2\zeta(1+2\zeta\xi)(\mathrm{Y}_3)^3\\ &+ M_1^2(\mathrm{Y}_2 + G) + Kp\mathrm{Y}_2 + (\mathrm{Y}_2)^2,\end{aligned} \tag{33}$$

$$\begin{aligned} Y_5' = &\left(\frac{1}{(1+2\zeta\xi)(1+\varepsilon Y_4)+\frac{4}{3}(1+2\zeta\xi)\mathrm{Rd}}\right) \\ &\times(-2\zeta(1+\varepsilon Y_4)Y_5-(1+2\zeta\xi)\varepsilon \\ &-\mathrm{Pr}(1+2\zeta\xi)(\mathrm{Nt}(Y_5)^2+\mathrm{Nb}Y_5Y_7) \\ &-\mathrm{Pr}(QY_4+Y_1Y_5)-\frac{4}{3}\zeta\mathrm{Rd}Y_5\Big), \end{aligned} \tag{34}$$

$$\begin{aligned} Y_7' = &\left(\frac{1}{(1+2\zeta\xi)}\right)\Big(-2\zeta Y_7-2\zeta\frac{\mathrm{Nt}}{\mathrm{Nb}}Y_5 \\ &-(1+2\zeta\xi)\frac{\mathrm{Nt}}{\mathrm{Nb}}Y_5'-\mathrm{Sc}Y_1Y_7 \\ &+\gamma_r\mathrm{Sc}(1+\delta Y_4)^m Y_6\exp^{\frac{-E_2}{(1+\delta Y_4)}}\Big), \end{aligned} \tag{35}$$

$$\begin{aligned} Y_9' = &\left(\frac{1}{(1+2\zeta\xi)}\right)(-2\zeta Y_9-\mathrm{Sb}Y_1Y_9+\mathrm{Pe}((1+2\zeta\xi) \\ &\times(Y_7Y_9+(\delta_1+Y_8)Y_7')+(\delta_1+Y_8)\zeta Y_7)), \end{aligned} \tag{36}$$

$$\begin{aligned} &Y_1(0)=0, \\ &Y_2(0)=1+h_1Y_3(0)\left(1+\frac{n-1}{2}\mathrm{We}^2(Y_3(0))^2\right), \\ &Y_2(\infty)=0, \end{aligned} \tag{37}$$

$$\begin{aligned} &Y_4(0)=1+u_1Y_5, \quad Y_4(\infty)=0, \\ &\mathrm{Nb}Y_7(0)+\mathrm{Nt}Y_5(0)=0, \\ &Y_6(\infty)=0, Y_8(\infty)=0, \quad Y_8(0)=1. \end{aligned} \tag{38}$$

The detailed about build-in scheme, initial guess, and convergence criteria are well explained by Ali *et al.* [49]. To observe the validity of present MATLAB code, we validate our current outcomes against already published numerical value for specific case. For ζ curvature distinct strength, it is reported that our code outcomes match with aforementioned studies. The present obtained outcomes are tested with the already existing literature [50,51] against the limited case and are found to be an excellent agreement, as indicated in Table 1. Therefore, we are confident that present findings are reliable and correct.

Table 1: When analysing the variation of $\frac{C_f(\mathrm{Re})^{-\frac{1}{2}}}{2}$ with different values of ζ, the following parameter values are considered: We = G = M_1 = Kp = h_1 = 0 and n = 1

ζ	Rangi et al. [50]	Hashim et al. [51]	Current result
0	−1.0000	−1.0000	−1.0000
0.25	−1.094378	−1.094373	−1.090845
0.5	−1.188715	−1.188727	−1.188672
0.75	−1.281833	−1.281819	−1.281823

5 Results and discussion

This section examines the influence of various key physical parameters involved in the problem, including the magnetic parameter (M), heat generation (Q), porosity (K_p), Weissenberg number (We), activation energy (E_2), radiation (Rd), Brownian motion (Nb), chemical reaction (γ_r), thermophoresis (Nt), Prandtl number (Pr), Schmidt number (Sc), microorganism difference dimensionless parameter (δ_1), dimensionless bioconvection Schmidt number (E_1), dimensionless Peclet number (Pe), Biot number (Bi), slip velocity (h_1), slip temperature (h_2), and temperature difference (δ), on fluid speed, temeprature, and concentration functions are analysed in detail. Table 2 illustrates how the C_f rises with ζ, permeability parameter, and has a negligible effect when n, M_1, We, and E are increased and diminishes as the slip parameter surges. Table 3 demonstrates that Nu_x increases with Pr, while it decreases with an increase in Rd, Q, h_2, ζ, and Nt parameters and has a negligible effect on Nu_x when the value of Brownian motion factor surges. Table 4 demonstrates that the Sh_x boosted with the Nt, Sc increased while it diminishing with an increment in ζ, Nb and negligible effect on Sh_x when increased γ_r, m, E_2, δ.

Table 2: Taking into account the impacts of various factors on the coefficient of skin friction when ε = 0.1, Rd = 0.8, Sc = E_2 = 0.2, δ = 0.2, γ_r = 0.8, m = 1.3, Nb = Q = 0.1, Sb = 0.5, Pe = δ_1 = 0.2, h_2 = Nt = 0.1, Pr = 7

ζ	M_1	We	n	E_2	Kp	h_1	$-\frac{C_f(\mathrm{Re})^{-\frac{1}{2}}}{2}$
0.2	0.1	0.1	0.5	0	0.1	0.1	0.976474
0.5	—	—	—	—	—	—	1.06186
0.7	—	—	—	—	—	—	1.11586
0.2	0.3	—	—	—	—	—	1.00852
—	0.5	—	—	—	—	—	1.0682
—	0.7	—	—	—	—	—	1.14919
—	0.1	0.1	—	—	—	—	0.976474
—	—	0.3	—	—	—	—	0.971673
—	—	0.5	—	—	—	—	0.961282
—	—	0.1	0.5	—	—	—	0.976474
—	—	—	0.7	—	—	—	0.976709
—	—	—	0.9	—	—	—	0.976942
—	—	—	0.5	0	—	—	0.976474
—	—	—	—	0.1	—	—	0.974657
—	—	—	—	0.2	—	—	0.97287
—	—	—	—	0	0.1	—	0.976474
—	—	—	—	—	0.3	—	1.05377
—	—	—	—	—	0.5	—	1.12318
—	—	—	—	—	0.1	0.1	0.976474
—	—	—	—	—	—	0.3	0.776998
—	—	—	—	—	—	0.5	0.650122

Table 3: Analysing the influence of multiple factors on the Nu_x when We = M_1 = h_2 = Kp = 0.1, n = 0.5, E = 0.1, h_1 = 0.1, E_2 = Sc = 0.2, δ = 0.2, γ_r = 0.8, Sb = 0.5, δ_1 = Pe = 0.2, m = 1.3

ζ	Nt	Nb	ε	Rd	Pr	Q	h_2	$-\theta(0)$
0.2	0.2	0.1	0.1	0.8	7	0.1	0.1	0.869277
0.4	—	—	—	—	—	—	—	0.84314
0.6	—	—	—	—	—	—	—	0.81526
0.2	0.2	—	—	—	—	—	—	0.869277
—	0.5	—	—	—	—	—	—	0.844893
—	0.7	—	—	—	—	—	—	0.828069
—	0.2	0.3	—	—	—	—	—	0.869277
—	—	0.5	—	—	—	—	—	0.869277
—	—	0.7	—	—	—	—	—	0.869277
—	—	0.1	0.1	—	—	—	—	0.869277
—	—	—	0.3	—	—	—	—	0.823928
—	—	—	0.5	—	—	—	—	0.783784
—	—	—	0.1	0.8	—	—	—	0.869277
—	—	—	—	1	—	—	—	0.800687
—	—	—	—	1.2	—	—	—	0.740961
—	—	—	—	0.8	5.5	—	—	0.742537
—	—	—	—	—	6.5	—	—	0.829494
—	—	—	—	—	6.8	—	—	0.853618
—	—	—	—	—	7	0.1	—	0.869277
—	—	—	—	—	—	0.3	—	0.393361
—	—	—	—	—	—	0.4	—	0.30945
—	—	—	—	—	—	0.1	0.1	0.869277
—	—	—	—	—	—	—	0.3	0.745021
—	—	—	—	—	—	—	0.5	0.577464

Table 4: Assessing the implications of various factors influencing the local Sherwood index when We = M_1 = Kp = 0.1, n = 0.5, E = 0.1, h_1 = 0.1, ε = 0.1, h_2 = 0.1, Pr = 7, Q = 0.2, Sb = δ_1 = Pe = 0.2, Rd = 0.8

ζ	Nb	Nt	Sc	γ_r	m	δ	E_2	$-\phi(0)$
0.2	0.5	0.4	0.2	0.8	1.3	0.2	0.2	0.677332
0.4	—	—	—	—	—	—	—	0.65419
0.6	—	—	—	—	—	—	—	0.629095
0.2	0.5	—	—	—	—	—	—	0.677332
—	0.7	—	—	—	—	—	—	0.483808
—	0.9	—	—	—	—	—	—	0.376296
—	0.5	0.4	—	—	—	—	—	0.677332
—	—	0.6	—	—	—	—	—	0.991908
—	—	0.8	—	—	—	—	—	1.28935
—	—	0.4	0.2	—	—	—	—	0.677332
—	—	—	0.4	—	—	—	—	0.991908
—	—	—	0.6	—	—	—	—	1.28935
—	—	—	0.2	0.8	—	—	—	0.677332
—	—	—	—	1	—	—	—	0.673225
—	—	—	—	1.2	—	—	—	0.669307
—	—	—	—	0.8	1.3	—	—	0.677332
—	—	—	—	—	1.5	—	—	0.668738
—	—	—	—	—	1.7	—	—	0.668159
—	—	—	—	—	1.3	0.2	—	0.677332
—	—	—	—	—	—	0.4	—	0.669307
—	—	—	—	—	—	0.6	—	0.669307
—	—	—	—	—	—	0.2	0.2	0.677332
—	—	—	—	—	—	—	0.4	0.673121
—	—	—	—	—	—	—	0.6	0.676453

Table 5: Taking into account the influence of various factors on motile microorganisms when We = M_1 = Kp = 0.1, n = 0.5, E = 0.1, h_1 = 0.1, h_2 = 0.1, ε = 0.1, Nt = 0.1, Q = 0.1, Rd = 0.8, Sc = E_2 = 0.2, δ = 0.2, γ_r = 0.8, m = 1.3, Nb = 0.1, Pr = 7

ζ	Sb	Pe	δ_1	$-\chi(0)$
0.2	0.9	0.2	0.2	0.390263
0.4	—	—	—	0.448539
0.6	—	—	—	0.521424
0.2	0.9	—	—	0.390263
—	1.2	—	—	0.65271
—	1.4	—	—	0.731399
—	0.9	0.2	—	0.390263
—	—	0.4	—	0.506205
—	—	0.6	—	0.491207
—	—	0.2	0.2	0.438326
—	—	—	0.4	0.38609
—	—	—	0.7	0.307736

In Table 5, the value of Nn_x surges as ζ and Sb increase and then diminishes as the Pe, and δ_1 increase.

Figure 2 exhibits the consequence ζ has on the velocity distribution. The ζ exhibits an adverse relationship with R. The radius of the cylinder declines with an enhancement in ζ. A contact area between the fluid and the boundary layer diminishes. As a result, the resistive force exerted by the fluid decreases, leading to a boost in velocity distribution. Figure 3 shows temperature profile is influenced by the ζ. ζ leads to an increase in the temperature distribution. Physically, for greater values of the curvature parameter, the cylinder's radius decreases, leading to a reduction in the surface area near the solid boundary. It is

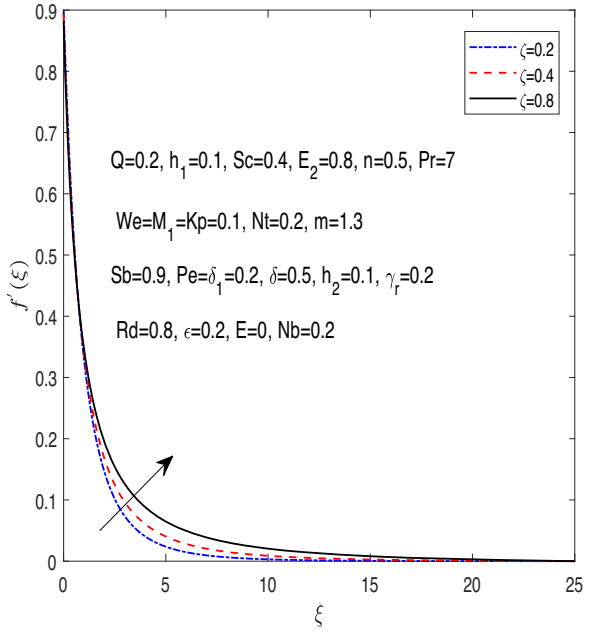

Figure 2: Velocity appearance against ζ.

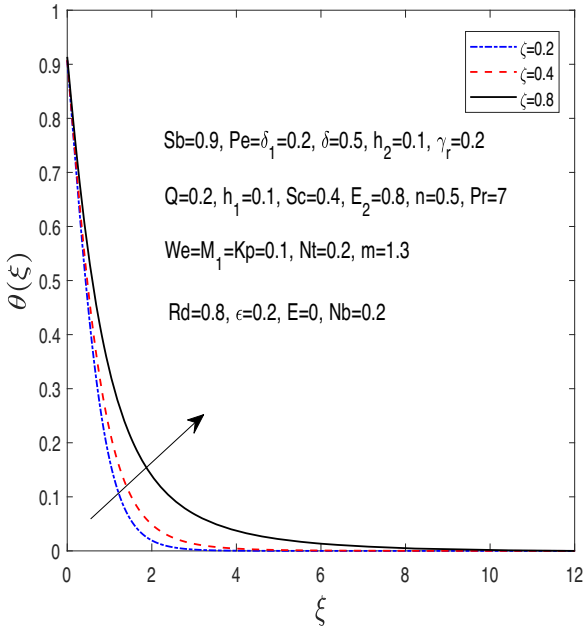

Figure 3: Temperature appearance against ζ.

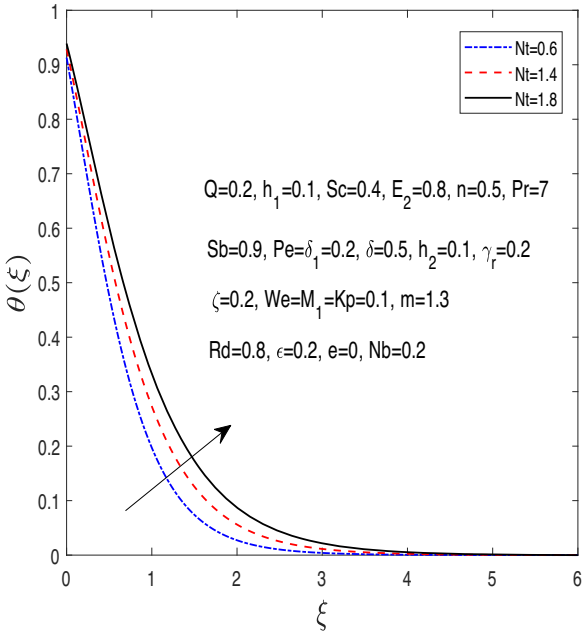

Figure 5: Temperature appearance against Nt.

important to highlight that heat transfer occurs in two modes: conduction at the surface and convection within the fluid domain. As the surface area of the cylinder diminishes, a slight decrease in the temperature profile is observed near the cylinder's surface. This occurs because a smaller amount of heat energy is conducted from the surface to the fluid. Simultaneously, the thermal boundary layer thickness increases due to enhanced heat transfer within the fluid, driven by the improved convection process around the cylinder. Figure 4 demonstrates concentration distribution is influenced by ζ. Concentration distribution dwindles when ζ has surged.

Figure 5 illustrates that increasing the values of Nt leads to temperature curves enhanced. Figure 6 shows that an enhanced Nt value results in a surge in the

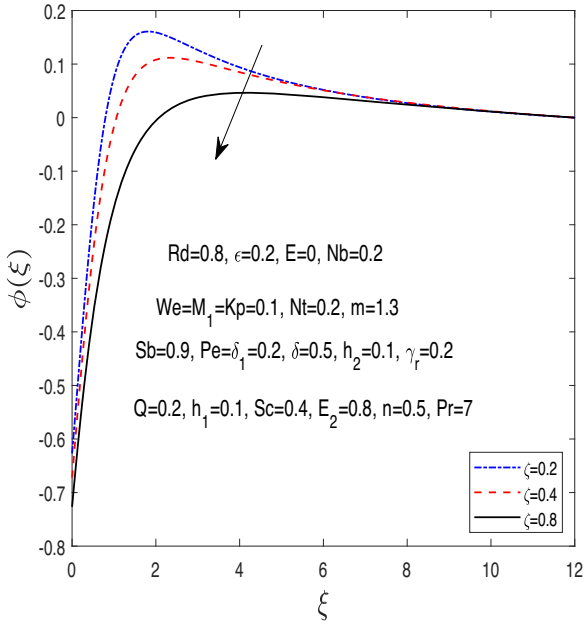

Figure 4: Concentration appearance against ζ.

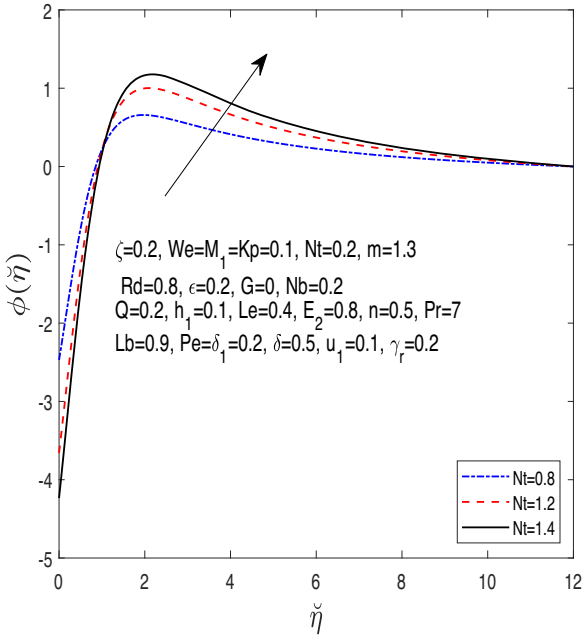

Figure 6: Concentration appearance against Nt.

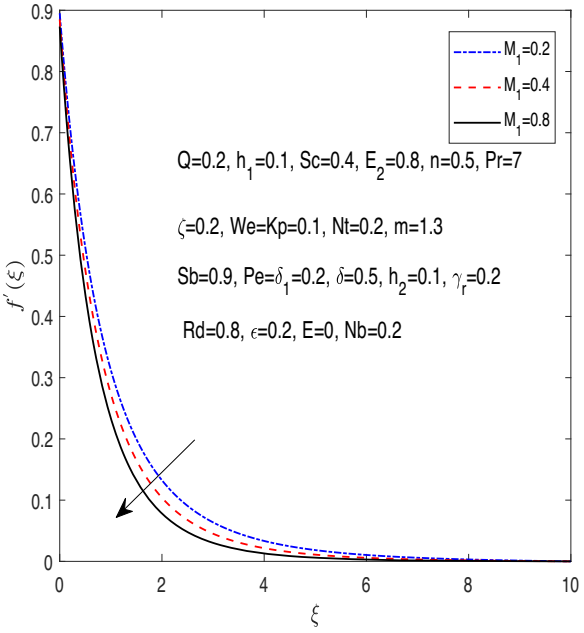

Figure 7: Velocity appearance against M_1.

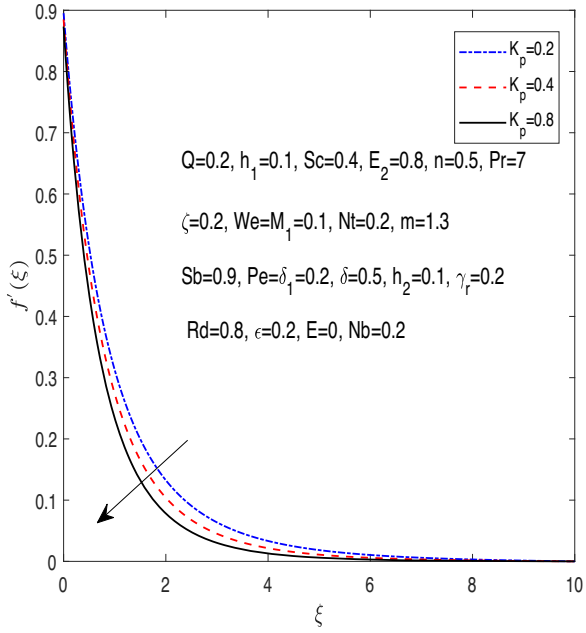

Figure 9: Velocity appearance against K_p.

concentration curve. Actually, the growing power of Nt, a larger number of nanoparticles migrate from the hot surface to the cold surface. This movement ultimately leads to an increase in both the temperature and concentration distributions. Figure 7 demonstrates that the velocity profile is primarily influenced by M_1. The Lorentz force arises from a change in M_1, leading to resistive forces that cause the fluid flow to reverse direction and reduce velocity. The velocity distribution diminishes as we boost h_1, as observed in Figure 8. It is noted that when slip occurs, the velocity near the stretching surface does not match the wall's stretching velocity. Under slip conditions, the momentum imparted by the stretching surface to the fluid is only partially transferred. This results in a reduction in fluid

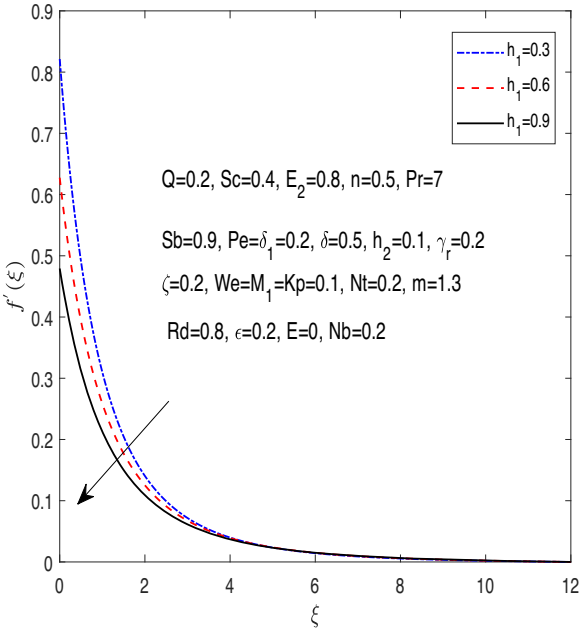

Figure 8: Velocity appearance against h_1.

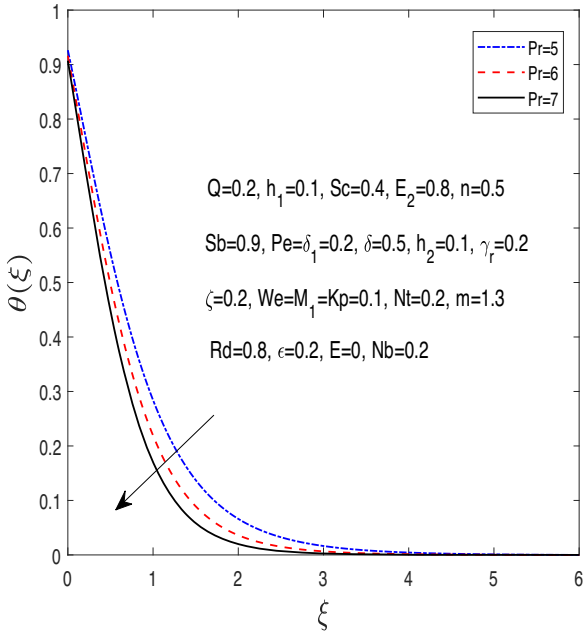

Figure 10: Temperature appearance against Pr.

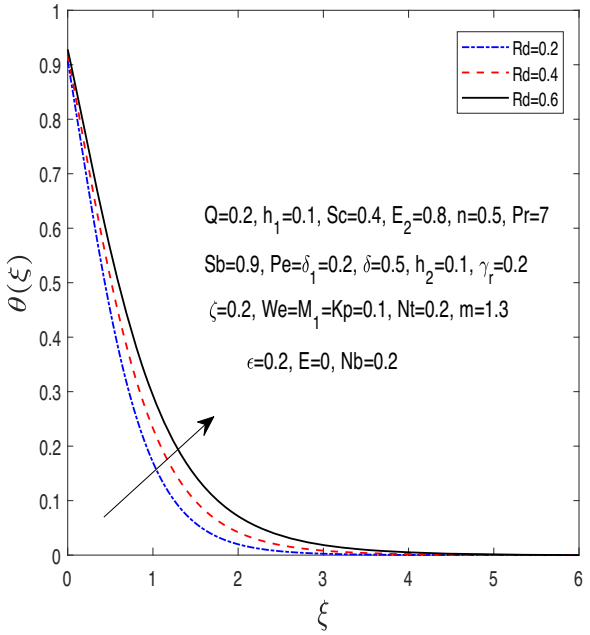

Figure 11: Temperature appearance against Rd.

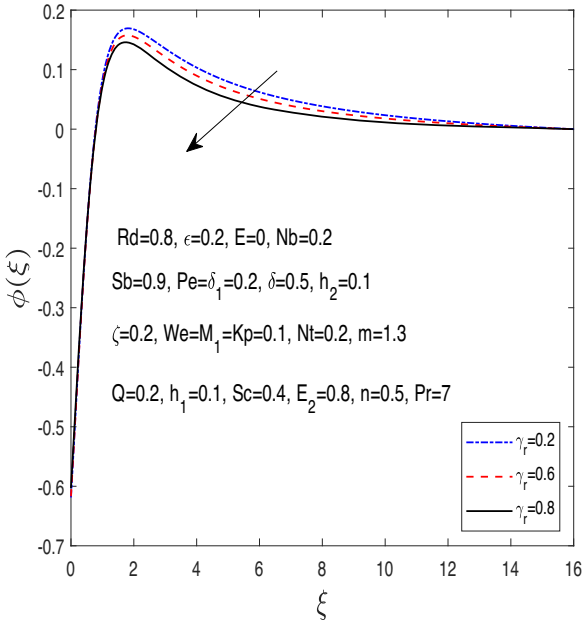

Figure 13: Concentration appearance against γ_r.

velocity, thereby causing a deceleration in the boundary layer flow. Figure 9 demonstrates that the *Kp* influences the velocity appearance. Distribution of velocity is diminished with enhanced *Kp*. The resistance to fluid flow, which arises due to permeable medium, is responsible for reduced velocity appearance. Figure 10 illustrates the impact of the Pr parameter on the temperature profile. Increasing Pr caused a reduction in the thermal boundary layer and a decrease in the temperature distribution.

Figure 11 demonstrates the influence of the radiation parameter. Fluid is heated by radiation, consequently resulting in an enhanced temperature curve. Physically, a more heat transfer is occur due to greater radiation values so temperature maximise. The temperature distribution diminishes as we boost h_2 parameter, as illustrated

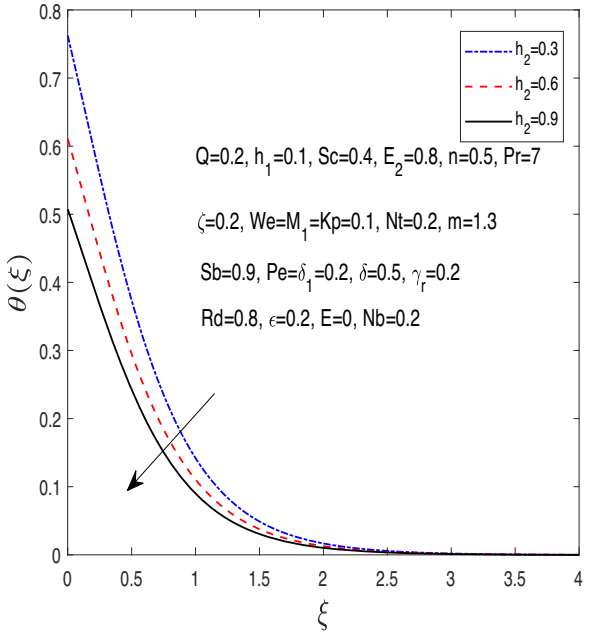

Figure 12: Temperature appearance against h_2.

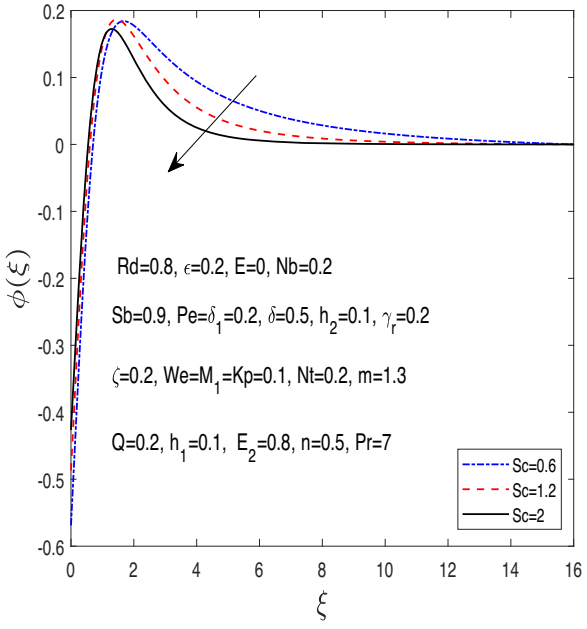

Figure 14: Concentration appearance against Sc.

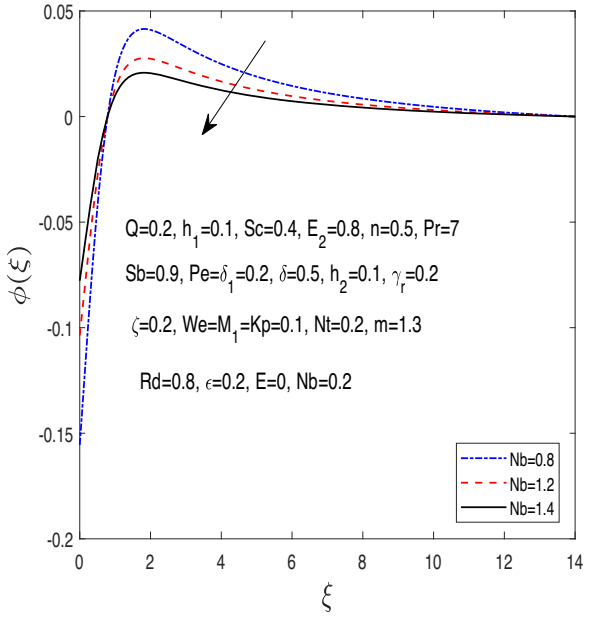

Figure 15: Concentration appearance against Nb.

in Figure 12. The impact of γ_r, Nb, and Sc on the concentration distribution is depicted in Figures 13–15, respectively. The graphs demonstrate that surging γ_r, Sc, and Nb values resulted in a dwindle in the concentration distribution. Physically, a rise in Nb leads to an increase in the random motion of nanoparticles. As the interaction among particles intensifies, kinetic energy is converted into thermal energy, resulting in a reduction in the nanoparticle concentration within the fluid. As the Sc strength increases, the weaker Brownian diffusion coefficient leads to a reduction in boundary layer thickness and a decline in $\phi(\xi)$. This is attributed to the influence of the increasing Brownian diffusion coefficient with higher Sc. Figure 16 indicates how the Sb influences the microorganism profile, with a boost in Sb leading to a reduction in the motile microorganism profile.

6 Conclusion

This investigation primary focus to analyses the slip flow of EMHD Carreau nanofluid across a stretching cylinder in the context of Arrhenius activation energy, chemical reactions, and variable thermal conductivity within a porous medium. The study explicitly considers the consequences of chemical reactions, the presence of a porous medium, and changes in thermal conductivity. Buongiorno's model is employed, and also, the effects of changing EMHD forces on fluid flow dynamics are investigated. By introducing nonsimilarity variables, the partial differential equations are transformed into a system of coupled ODEs. The *bvp4c* solver, a MATLAB built-in solver, is implemented to compute the solution to the resultant set of ODEs. The outcomes of present report would be beneficial in the fluids, which

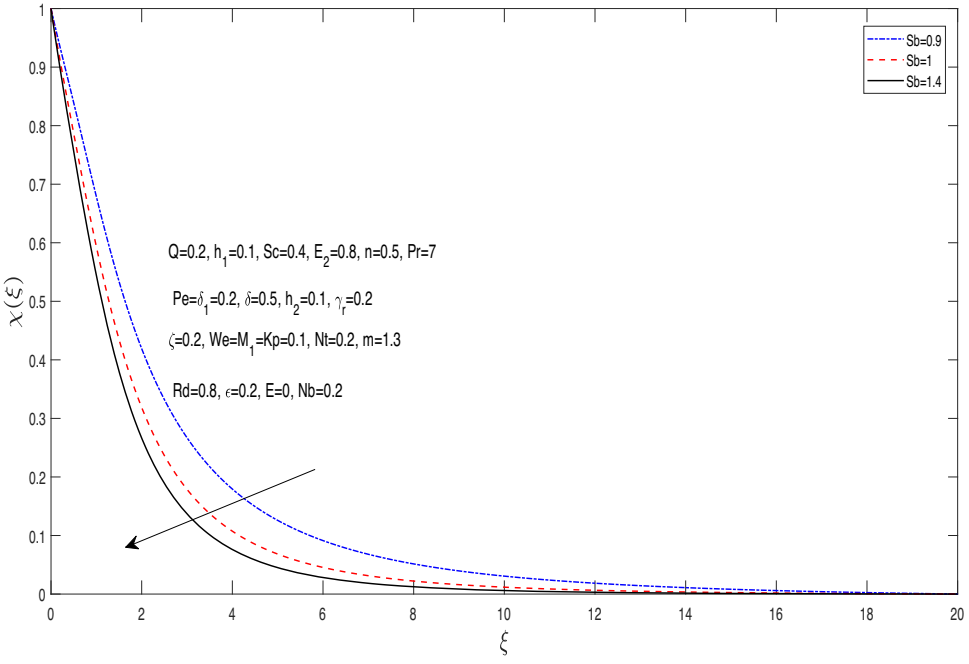

Figure 16: Microorganism appearance against Sb.

are designed for optimisation of heat transfer in various industrial zone and processing material. The present study main finding points are shown below:

- The velocity profile dwindles as the porosity (Kp) and magnetic (M_1) values increase and rises as the curvature strength (ζ) value rises.
- The temperature profile rises with the value of curvature (ζ), and radiation (Rd) rises and falls as the values of Pr, u_1, and Nb rise. The enhancing power of radiation, thermophoresis, and heat source are cause to Nn_x decreases, but reverse trend is reported for Pr.
- As the ζ, γ_r, Sc, and Nb values rise, the concentration profile dwindles and increases as do the Nt and E parameter values.
- As Nb and ζ increase the Sh_x falls, but when the Nt value rises, it increases. As Sb and ζ values increased, the result in motile microorganisms rise.

For future study, it can be extended further to optimise the host fluid temperature of different models like Casson, Ellis, Maxwell, and micropolar. In addition, these models can be expanded to incorporate hybrid nanoparticles for enhanced performance.

Funding information: The authors state no funding involved.

Author contributions: All authors have accepted responsibility for the entire content of this manuscript and approved its submission. Conceptualization; Muhammad Afzal, Imran Siddique, Mohammed M. M. Jaradat and Bagh Ali. Methodology; Imran Siddique and Badar E Alam, Funding acquisition; Mohammed M. M. Jaradat. Investigation; Bagh Ali. Validation; Binjian Ma. Data curation; Badar E Alam and Faiza Zahid. Writing – original draft preparation; Faiza Zahid and Bagh Ali. Software; Bagh Ali and Mohammed M. M. Jaradat. Writing – review and editing; Muhammad Afzal, Imran Siddique and Bagh Ali. Supervision; Binjian Ma.

Conflict of interest: The authors state no conflict of interest.

Data availability statement: The datasets generated and/or analysed during the current study are available from the corresponding author on reasonable request.

References

[1] Sharma BK, Kumar A, Gandhi R, Bhatti M. Exponential space and thermal-dependent heat source effects on electro-magneto-hydrodynamic Jeffrey fluid flow over a vertical stretching surface. Int J Modern Phys B. 2022;36(30):2250220.

[2] Hashim, Hamid A, Khan M. Transient flow and heat transfer mechanism for Williamson-nanomaterials caused by a stretching cylinder with variable thermal conductivity. Microsyst Tech. 2019;25:3287–97.

[3] Senbagaraja P, De P. Dual solution of EMHD Tangent hyperbolic nanofluid with viscous dissipation and suction. Int J Fluid Mech Res. 2024;51(4):17–41.

[4] Carreau PJ. Rheological equations from molecular network theories. Trans Soc Rheol. 1972;16(1):99–127.

[5] Gomathi N, De P. Impact of hall currents and ion slip on mixed convective Casson Williamson nanofluid flow with viscous dissipation through porous medium. Nanosci Tech Int J. 2024;15(1):65–86.

[6] Raju C, Sandeep N. Falkner-Skan flow of a magnetic-Carreau fluid past a wedge in the presence of cross diffusion effects. Europ Phys J Plus. 2016;131:1–13.

[7] Shah Z, Asghar A, Ying TY, Lund LA, Alshehri A, Vrinceanu N. Numerical investigation of sodium alginate-alumina/copper radiative hybrid nanofluid flow over a power law stretching/shrinking sheet with suction effect: a study of dual solutions. Results Eng. 2024;21:101881.

[8] Fadhel MA, Asghar A, Lund LA, Shah Z, Vrinceanu N, Tirth V. Dual numerical solutions of Casson SA-hybrid nanofluid toward a stagnation point flow over stretching/shrinking cylinder. Nanotech Rev. 2024;13(1):20230191.

[9] Yasmin H, Mahnashi AM, Hamali W, Lone SA, Raizah Z, Saeed A. A numerical analysis of the blood-based Casson hybrid nanofluid flow past a convectively heated surface embedded in a porous medium. Open Phys. 2024;22(1):20230193.

[10] Yasmin H, Shahab S, Lone SA, Raizah Z, Saeed A. Convective flow of a magnetohydrodynamic second-grade fluid past a stretching surface with Cattaneo-Christov heat and mass flux model. Open Phys. 2024;22(1):20230204.

[11] Kumar A, Sharma BK, Gandhi R, Mishra NK, Bhatti M. Response surface optimisation for the electromagnetohydrodynamic Cu-polyvinyl alcohol/water Jeffrey nanofluid flow with an exponential heat source. J Magnetism Magnetic Materials. 2023;576:170751.

[12] Raju C, Sandeep N. Unsteady three-dimensional flow of Casson-Carreau fluids past a stretching surface. Alexandr Eng J. 2016;55(2):1115–26.

[13] Khan M, Azam M, Munir A. On unsteady Falkner-Skan flow of MHD Carreau nanofluid past a static/moving wedge with convective surface condition. J Mol Liquids. 2017;230:48–58.

[14] Gandhi R, Sharma B, Khanduri U. Electromagnetohydrodynamics Casson pulsatile nanofluid flow through a bifurcated stenosed artery: Magnetically targeted drug delivery. J Appl Phys. 2023;134(18):184701.

[15] Abdal S, Mariam A, Ali B, Younas S, Ali L, Habib D. Implications of bioconvection and activation energy on Reiner-Rivlin nanofluid transportation over a disk in rotation with partial slip. Chin J Phys. 2021;73:672–83.

[16] Ali L, Wu YJ, Ali B, Abdal S, Hussain S. The crucial features of aggregation in TiO2-water nanofluid aligned of chemically comprising microorganisms: A FEM approach. Comput Math Appl. 2022;123:241–51.

[17] Kumar Sharma B, Gandhi R. Entropy-driven optimisation of radiative Jeffrey tetrahybrid nanofluid flow through a stenosed bifurcated artery with Hall effects. Phys Fluids. 2023;35(12):121903.

[18] Choi SU, Eastman JA. Enhancing thermal conductivity of fluids with nanoparticles. Argonne National Lab.(ANL), Argonne, IL (United States); 1995.
[19] Choi S, Zhang ZG, Yu W, Lockwood F, Grulke E. Anomalous thermal conductivity enhancement in nanotube suspensions. Appl Phys Lett. 2001;79(14):2252–4.
[20] Rajeswari PM, De P. Multi-stratified effects on stagnation point nanofluid flow with gyrotactic microorganisms over porous medium. J Porous Media. 2024;27(5):67–84.
[21] Yasmin H, Lone SA, Alrabaiah H, Raizah Z, Saeed A. A numerical investigation of the two-dimensional magnetohydrodynamic water-based hybrid nanofluid flow composed of Fe3O4 and Au nanoparticles over a heated surface. Nanotech Rev. 2024;13(1):20240010.
[22] Kuznetsov AV. Nanofluid bioconvection in water-based suspensions containing nanoparticles and oxytactic microorganisms: oscillatory instability. Nanoscale Res Lett. 2011;6:1–13.
[23] Chan SQ, Aman F, Mansur S. Sensitivity analysis on thermal conductivity characteristics of a water-based bionanofluid flow past a wedge surface. Math Problems Eng. 2018;2018(1):9410167.
[24] Sparrow E, Cess R. The effect of a magnetic field on free convection heat transfer. Int J Heat Mass Transfer. 1961;3(4):267–74.
[25] Mazumder B, Gupta A, Datta N. Hall effects on combined free and forced convective hydromagnetic flow through a channel. Int J Eng Sci. 1976;14(3):285–92.
[26] Raptis A. Flow through a porous medium in the presence of a magnetic field. Int J Energy Res. 1986;10(1):97–100.
[27] Rudraiah N, Barron R, Venkatachalappa M, Subbaraya C. Effect of a magnetic field on free convection in a rectangular enclosure. Int J Eng Sci. 1995;33(8):1075–84.
[28] AboEldahab EM. Radiation effect on heat transfer in an electrically conducting fluid at a stretching surface with a uniform free stream. J Phys D Appl Phys. 2000;33(24):3180.
[29] Awais M, Malik M, Bilal S, Salahuddin T, Hussain A. Magnetohydrodynamic (MHD) flow of Sisko fluid near the axisymmetric stagnation point towards a stretching cylinder. Results Phys. 2017;7:49–56.
[30] Sharma BK, Kumawat C, Khanduri U, Mekheimer KS. Numerical investigation of the entropy generation analysis for radiative MHD power-law fluid flow of blood through a curved artery with Hall effect. Waves Random Complex Media. 2023:1–38. doi: 10.1080/17455030.2023.2226228.
[31] Wakif A, Chamkha A, Animasaun I, Zaydan M, Waqas H, Sehaqui R. Novel physical insights into the thermodynamic irreversibilities within dissipative EMHD fluid flows past over a moving horizontal riga plate in the coexistence of wall suction and joule heating effects: a comprehensive numerical investigation. Arab J Sci Eng. 2020;45:9423–38.
[32] Sajid M, Hayat T. Influence of thermal radiation on the boundary layer flow due to an exponentially stretching sheet. Int Commun Heat Mass Transfer. 2008;35(3):347–56.
[33] Shehzad SA, Alsaedi A, Hayat T, Alhuthali MS. Three-dimensional flow of an Oldroyd-B fluid with variable thermal conductivity and heat generation/absorption. PloS One. 2013;8(11):e78240.
[34] Waqas M, Khan MI, Hayat T, Alsaedi A, Khan MI. On Cattaneo-Christov double diffusion impact for temperature-dependent conductivity of Powell-Eyring liquid. Chin J Phys. 2017;55(3):729–37.
[35] Dogonchi A, Ganji D. Convection-radiation heat transfer study of moving fin with temperature-dependent thermal conductivity, heat transfer coefficient and heat generation. Appl Thermal Eng. 2016;103:705–12.
[36] Akbar NS, Tripathi D, Khan ZH, Bég OA. A numerical study of magnetohydrodynamic transport of nanofluids over a vertical stretching sheet with exponential temperature-dependent viscosity and buoyancy effects. Chem Phys Lett. 2016;661:20–30.
[37] Song J, Liu Z, Ma Z, Zhang J. Experimental investigation of convective heat transfer from sewage in heat exchange pipes and the construction of a fouling resistance-based mathematical model. Energy Buildings. 2017;150:412–20.
[38] Khan M, Malik M, Salahuddin T, Rehman K, Naseer M, et al. MHD flow of Williamson nanofluid over a cone and plate with chemically reactive species. J Mol Liquids. 2017;231:580–8.
[39] Sobamowo M, Yinusa A, Oluwo A. Finite element analysis of flow and heat transfer of dissipative Casson-Carreau nanofluid over a stretching sheet embedded in a porous medium. Aeron Aero Open Access J. 2018;2(5):294–308.
[40] Akbar N, Nadeem S, Haq RU, Ye S. MHD stagnation point flow of Carreau fluid toward a permeable shrinking sheet: Dual solutions. Ain Shams Eng J. 2014;5(4):1233–9.
[41] Khan M, Azam M, Alshomrani A. Effects of melting and heat generation/absorption on unsteady Falkner-Skan flow of Carreau nanofluid over a wedge. Int J Heat Mass Transfer. 2017;110:437–46.
[42] Hsiao KL. To promote radiation electrical MHD activation energy thermal extrusion manufacturing system efficiency by using Carreau-Nanofluid with parameters control method. Energy. 2017;130:486–99.
[43] Ali L, Wang Y, Ali B, Liu X, Din A, Al Mdallal Q. The function of nanoparticleas diameter and Darcy-Forchheimer flow over a cylinder with effect of magnetic field and thermal radiation. Case Stud Thermal Eng. 2021;28:101392.
[44] Shah SAA, Ahammad NA, Ali B, Guedri K, Awan AU, Gamaoun F, et al. Significance of bio-convection, MHD, thermal radiation and activation energy across Prandtl nanofluid flow: A case of stretching cylinder. Int Commun Heat Mass Transfer. 2022;137:106299.
[45] Ali B, Siddique I, Khan I, Masood B, Hussain S. Magnetic dipole and thermal radiation effects on hybrid base micropolar CNTs flow over a stretching sheet: Finite element method approach. Results Phys. 2021;25:104145.
[46] Awan AU, Ali B, Shah SAA, Oreijah M, Guedri K, Eldin SM. Numerical analysis of heat transfer in Ellis hybrid nanofluid flow subject to a stretching cylinder. Case Stud Thermal Eng. 2023;49:103222.
[47] Mishra A, Kumar M. Velocity and thermal slip effects on MHD nanofluid flow past a stretching cylinder with viscous dissipation and Joule heating. SN Appl Sci. 2020;2(8):1350.
[48] Sharif H, Habib D, Ali B, et al. Bejan number and entropy generation analysis of unsteady MHD non-Newtonian micropolar squeezed trihybrid nanofluid flow. Partial Differ Equ Appl Math. 2024;10:100703.
[49] Ali B, Sharif H, Habib D, Ghazwani HA, Saman I, Yang H. Significance of tri-hybrid nanoparticles in thermal management subject to magnetized squeezing flow of a Boger-micropolar nanofluid between concentring disks. J Mol Liquids. 2024;397:124141.
[50] Rangi RR, Ahmad N. Boundary layer flow past a stretching cylinder and heat transfer with variable thermal conductivity. Appl Math. 2012;3(3):1–5.
[51] Hashim, Khan M, Saleh Alshomrani A. Characteristics of melting heat transfer during flow of Carreau fluid induced by a stretching cylinder. Europ Phys J E. 2017;40:1–9.